

See discussions, stats, and author profiles for this publication at: <https://www.researchgate.net/publication/225067233>

Solvent Effects on the Thermal and Mechanical Properties of Poly(methyl methacrylate) Casted from Concentrated Solutions

ARTICLE *in* ADVANCES IN POLYMER TECHNOLOGY · MARCH 2011

Impact Factor: 1.05 · DOI: 10.1002/adv.20203

CITATIONS

12

READS

354

3 AUTHORS, INCLUDING:



Niranjan Patra

Imperial College London

36 PUBLICATIONS 289 CITATIONS

SEE PROFILE

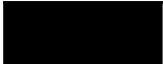


Marco Salerno

Istituto Italiano di Tecnologia

111 PUBLICATIONS 1,908 CITATIONS

SEE PROFILE



Solvent Effects on the Thermal and Mechanical Properties of Poly(methyl methacrylate) Casted from Concentrated Solutions

NIRANJAN PATRA

*University of Genova, viale Causa 13, I-16145 Genova, Italy
Italian Institute of Technology, via Morego 30, I-16163 Genova, Italy*

ALBERTO C. BARONE, MARCO SALERNO

Italian Institute of Technology, via Morego 30, I-16163 Genova, Italy

Received: March 17, 2010

Accepted: November 18, 2010

ABSTRACT: The thermal, mechanical, and structural properties of poly(methyl methacrylate) (PMMA) samples casted from solutions of chloroform, toluene, and *N,N*-dimethylformamide (DMF) were investigated by means of differential scanning calorimetry, nanoindentation, and Fourier transform infrared spectroscopy, respectively. The thermal analysis showed that for PMMA prepared from chloroform and toluene solutions the glass transition temperature was quite lower than for bulk PMMA, whereas for PMMA prepared from the DMF solution it was higher. The mechanical analysis showed higher reduced modulus and lower creep effect for PMMA prepared from the DMF solution than for PMMA prepared from the chloroform and toluene solutions. The spectroscopic analysis pointed out the formation of a strong bond between the polymer carbonyl group and the solvent amide group for the PMMA prepared

Correspondence to: Niranjan Patra; e-mail: niranjan.patra@iit.it.

from the DMF solution and a significant distortion of the polymer chain for the PMMA prepared from the chloroform and toluene solutions. Therefore, the observed thermal and mechanical behavior is ascribed to the different hydrogen bonding contributions, the rotation of the end group, and the distortion of the polymer chain. © 2011 Wiley Periodicals, Inc. *Adv Polym Techn* 30: 12–20, 2011; View this article online at wileyonlinelibrary.com. DOI 10.1002/adv.20203

KEY WORDS: PMMA; solvent; glass transition; modulus

Introduction

Past research on polymeric materials has mainly focused on the rheological behavior of their surfaces during dynamic processing and on the mechanical properties of the final products.^{1–3} Relatively little attention has been paid so far to the structural changes in the polymers when prepared by solvent casting. However, both optical properties⁴ of polymer samples casted from solutions and their morphology and mechanical properties can differ depending on the used solvent.⁵ In this perspective, the aim of the present work is to investigate the thermal, mechanical, and structural properties of samples obtained by casting poly(methyl methacrylate) (PMMA) prepared from different solvents, namely chloroform, toluene, and *N,N*-dimethylformamide (DMF) and let to dry in ambient air at room temperature.

PMMA is a thermoplastic polymer commonly employed as the main component of positive resists for both electron and UV photolithography,^{6,7} as well as an imprintable material for hot-embossing soft lithography.⁸ Because of its excellent transparency in the visible spectrum, PMMA is widely used in optical applications, especially as a matrix for nonlinear optical composite materials.^{9,10}

PMMA samples casted from solutions of different solvents have been extensively studied in the literature, to elucidate how the solvent affects the polymer. Briscoe et al. investigated the stiffness and hardness of PMMA films casted from chloroform, toluene, and carbon tetrachloride, finding lower values for the latter solvent.⁵ Bistac and Schultz¹¹ considered the effect of chloroform and toluene on the temperature of the α -relaxation for bulk PMMA and drop casted films, explaining the difference as an acid–base interaction between the basic sites of PMMA and the acid character of the solvent. Feng

et al.¹² applied an ultrasonic field to nascent PMMA films obtained by drop casting and found that the ultrasonic vibration decreased the amount of residual solvent in the film to one-twelfth of the value that occurs by spontaneous evaporation. Other studies focused on the effect of DMF and tetrahydrofuran on the miscibility in the liquid phase between PMMA and polyvinyl chloride at different relative concentrations,¹³ and the effect of solvents on the morphology of films prepared by either laser evaporation¹⁴ or drop casting.¹⁵

However, little information is reported in the literature about the thermal and mechanical behavior of PMMA obtained by solvent evaporation from PMMA-casted concentrated solutions. In this work, PMMA samples produced from different solvents were investigated experimentally using differential scanning calorimetry (DSC), nanoindentation, and Fourier transformed infrared spectroscopy (FTIR) to examine their thermal (i.e., glass transition), mechanical (i.e., reduced moduli and creep), and structural properties (i.e., bonding type and occurrence), respectively. Chloroform, toluene, and DMF were selected as the solvents to be tested, depending on their order by increasing polarity and hydrogen bonding contribution.¹⁶

Experimental

MATERIALS AND PROPERTIES

PMMA of $M_w \sim 120$ kg/mol in powder form, toluene, chloroform, and DMF of analytical grade were purchased from Sigma-Aldrich (Milan, Italy) and used without further purification.

To predict and characterize the mechanism of the dissolution of different molecular species one from another, the Hansen solubility parameters, which

TABLE I
Hansen Solubility Parameters of the Considered Compounds,¹⁶ with the Respective Distance R_a in the Hansen Space from PMMA

Name	Molecular Formulae	δ_d (MPa ^{0.5})	δ_p (MPa ^{0.5})	δ_h (MPa ^{0.5})	R_a (MPa ^{0.5})
Chloroform	CHCl ₃	17.8	3.1	5.7	7.78
Toluene	C ₆ H ₅ CH ₃	18.0	1.4	2.0	10.70
DMF	HCON(CH ₃) ₂	17.4	13.7	11.3	5.52
PMMA	(CH ₂ C(CH ₃)CO ₂ CH ₃) _n	18.6	10.5	7.5	–

describe their mutual molecular interactions, can be employed.¹⁶ The nominal values of these parameters for both the PMMA and the solvents used in the present study are presented in Table I. The parameters δ_d , δ_p , and δ_h represent the dispersion bonds, the polar bonds, and the hydrogen bonds, respectively. The closer the respective parameters are for the considered species, the smoother is the resulting solution, according to the equation for the distance R_a in the three-dimensional topological Hansen parameter space, defined as

$$R_a = [4(\delta_{d2} - \delta_{d1})^2 + (\delta_{p2} - \delta_{p1})^2 + (\delta_{h2} - \delta_{h1})^2]^{1/2} \quad (1)$$

SAMPLE PREPARATION

The PMMA powder was first dissolved in the three different solvents considered, with the same PMMA wt./vol. concentration of 200 mg/mL. The mixture was shaken and ultrasonicated at room temperature until the polymer appeared to be completely dissolved (i.e., the resulting solution looked optically clear).

The PMMA samples for the DSC and the FTIR analysis were prepared by drying PMMA solutions prepared from different solvents at room temperature for 4 days.

The PMMA samples for the nanoindentation were prepared by spin casting the PMMA solutions on clean glass substrates at 1000 rpm for 60 s (spinner SM-180-BT, Sawatec, Germany). Spin casting was used because in nanoindentation the sample surface comes in physical contact with the indenter tip, and for relatively low indentation depth the surface roughness may affect the results. The film thickness as measured by a XP-2 profilometer (AMBIO Technology, Santa Cruz, CA) was about 4 μm . The root mean square (RMS) roughness of the film surface as measured by atomic force microscopy on scan areas of $10 \times 10 \mu\text{m}^2$ was typically 4–8 nm.

The prepared samples were stored in a desiccator and measured twice for each technique, after 7 and 30 days from preparation, without observing significant variations. In the section Results and Discussion, the results of the first measurement for each technique are presented. In the following, the PMMA samples produced from solutions of different solvents will be termed shortly as PMMA/solvent.

THERMAL ANALYSIS

The DSC analysis was carried out on a Pyris Diamond SII instrument (Perkin-Elmer, Waltham, MA), operating in a nitrogen atmosphere at a flow rate of 10 mL/min. The instrument was calibrated using indium and zinc as standard materials. The PMMA samples were 7–8 mg by weight in all the measurements. The temperature was swept between 50 and 150°C, with a heating and cooling rate of 10°C/min. Each temperature scanning was repeated for three cycles. The glass transition temperature T_g was obtained at the inflection point of the jump heat flow.

NANOINDENTATION

The nanoindentation experiments were performed by using a NanoTest system (Micro Materials Ltd., Wrexham, UK) equipped with a Berkovich indenter tip¹⁷ with a nominal radius of curvature of ~ 50 nm, elastic modulus $E_t = 1141$ GPa, and Poisson's coefficient $\nu_t = 0.07$. To obtain an accurate indenter area function and to correct for the instrument compliance,^{18,19} the system was calibrated by iterative cycles of indentations into synthetic fused silica, with peak loads ranging from 0.5 to 200 mN. The experiments were performed in a cabinet-controlled temperature of $(22 \pm 0.1)^\circ\text{C}$, in mechanical and electrical low-noise conditions (signal vibration level RMS <10 mV). The indentations were load controlled and performed with loading and unloading

rate of 0.01 and 0.02 mN/s, respectively, with a 60-s dwell period at peak load, and varying the peak load in a range of 0.15–0.40 mN, chosen such that the indentation size effect and the tip effect at the low load limit were minimized, and the influence of the glass substrate at the high load limit was negligible.¹⁸ In fact, since for the peak loads in the selected range the indentation depths were all above 110 nm, the low surface roughness observed on the film top (4–8 nm RMS; see the section Sample Preparation) had no effect on our results. For each load, the indentations were repeated 10 times on different regions of the film surface.

FTIR ANALYSIS

The FTIR spectra of PMMA were acquired in the range of 400–4000 cm^{-1} on a VERTEX 70 instrument (Bruker, Madison, WI). The samples were analyzed in attenuated total reflection configuration, with an aperture diameter of 3 mm and a spectral resolution of 4 cm^{-1} . For an optimal signal-to-noise ratio, 50 scans were averaged per sample spectrum and apodized by applying the Happ–Genzel correction function for the Fourier transformation. The interferograms were corrected using a zero-filling factor of 2. All the spectra were baseline corrected by third-order polynomial and were normalized thereafter.

Results and Discussion

THERMAL BEHAVIOR

Figure 1a shows the DSC heating curves of three cycles for the “as received” PMMA powder. A wide exothermic peak at the first heating cycle appears at about 72°C. This peak can be ascribed to water absorbed by the PMMA, which is a quite hygroscopic material; it disappears, as expected, in the subsequent heating cycle, due to the release of the adsorbed water molecules.

In all the three cycles, a peak corresponding to the glass transition temperature T_g of PMMA appears around 100°C. In the second and third heating cycles, the T_g increases slightly, due to the condensed structure of the polymer, which after each melting spontaneously reassembles into a slightly more stable configuration. The final value observed in the third cycle ($\sim 104^\circ\text{C}$) is close to the nominal value reported in the data sheets of the manufacturer (105°C).

In Fig. 1b, the DSC analysis of a PMMA/chloroform sample is presented. In this case, no glass transition temperature appears in the first heating cycle. Instead, a broad exothermic peak is observed at $\sim 123^\circ\text{C}$. This peak can be due to the presence of residual solvent trapped with restricted molecular mobility inside the polymer matrix. Some solvent molecules are probably activated during the heating, and the respective Cl atoms react with the PMMA macroradicals instead of escaping from the polymer cage.

The second DSC heating curve in Fig. 1b shows a typical glass transition shoulder, but at a significantly lower temperature ($\sim 74^\circ\text{C}$) with respect to the bulk PMMA observed in Fig. 1a. Probably most of the residual solvent has already disappeared during the first cycle, but the reactions observed in that cycle have changed the structural characteristics of the PMMA. However between the second and the third scans the T_g increases significantly ($\sim 82^\circ\text{C}$), indicating that during the two subsequent cycles of the heat treatment the material is still settling to a different state of entanglement.

In Fig. 1c, the DSC analysis of a PMMA/toluene sample is presented. The first curve exhibits a glass transition at quite low temperature ($\sim 57^\circ\text{C}$) and shows some more features at much higher temperatures ($\sim 140^\circ\text{C}$). The latter features are not as strong and regularly shaped as the band observed for PMMA/chloroform at $\sim 123^\circ\text{C}$. They can probably be due to the relief of internal stresses in PMMA, occurring on the removal of the solvent during the first cycle. Similarly, the increase in T_g between second and third scans is also much lower (from $\sim 75^\circ\text{C}$ to $\sim 77^\circ\text{C}$) than in Fig. 1b. Both effects are probably associated with a weaker interaction between residual toluene molecules and PMMA, with respect to the case of chloroform. This result is supported by the value of R_a distance of PMMA from the different solvents, which is larger for toluene (~ 10.7) than for chloroform (~ 7.8).

Finally, in Fig. 1d, the DSC analysis of a PMMA/DMF sample is reported. Similarly to the PMMA/toluene sample (Fig. 1c), the first heating curve shows irregular features on the high-temperature end, assigned to PMMA–solvent interactions. However, these features are significantly more prominent than those in Fig. 1c. Both from the marked features of the first heating curve in Fig. 1d and from the R_a value of PMMA–solvent distance in case of DMF (~ 5.5), which is even lower than for chloroform (~ 7.8 , see Table I), it can be affirmed that the PMMA–solvent interaction is stronger in

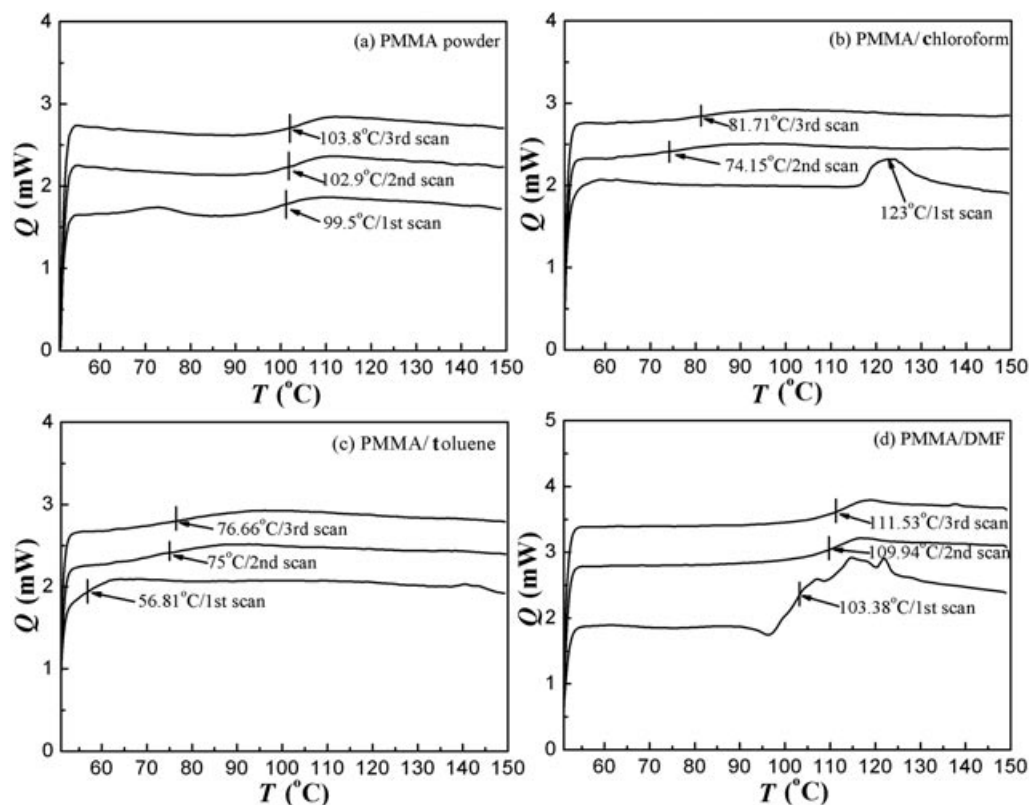


FIGURE 1. DSC thermal traces, acquired in three subsequent heating–cooling cycles for (a) the as received PMMA powder and the PMMA films prepared from three different solvents considered, (b) PMMA/chloroform, (c) PMMA/toluene, and (d) PMMA/DMF.

this case. This behavior could be ascribed to the replacement of the methoxy groups of PMMA by the amide groups of DMF during the first thermal cycle with formation of strong hydrogen bonds in the PMMA chains (see FTIR Analysis). This strong bonding is confirmed by values of T_g observed in the second and third scans, after that the PMMA structural of the first cycle has completed, which are the highest of all the solvents ($\sim 112^\circ\text{C}$) and even significantly higher than for the bulk PMMA (see Fig. 1a). As a consequence, the glass transition region falls in the same temperature window of the irregular PMMA–solvent interaction features of the first heating curve ($110\text{--}125^\circ\text{C}$). This overlap partly also hinders the presence of a T_g inflection point in the first curve, as shown in the figure.

MECHANICAL BEHAVIOR

Among the mechanical parameters commonly measured via instrumented nanoindentation, in this

work particular relevance is ascribed to the reduced modulus and the creep.

The reduced modulus, E_r , depends on both the specimen and the indenter materials according to the Hertzian theory of the elastic contact:

$$\frac{1}{E_r} = \frac{1 - \nu_s^2}{E_s} + \frac{1 - \nu_t^2}{E_t} \quad (2)$$

where E_s , ν_s and E_t , ν_t are the elastic moduli and Poisson's coefficients of specimen and tip material, respectively. The PMMA indentations of the spin-casted samples were performed with different peak loads L_{\max} within the aforementioned $0.15\text{--}0.40\text{ mN}$ maximum load range (see the section Thermal Analysis). Data points were obtained by averaging data sets of 10 indentations performed in each peak load at different regions.

The measured values of E_r for each type of sample (Fig. 2) are roughly constant within the whole range of peak loads, which demonstrates a good homogeneity of the samples. As a confirmation, atomic force microscope images of the different freshly

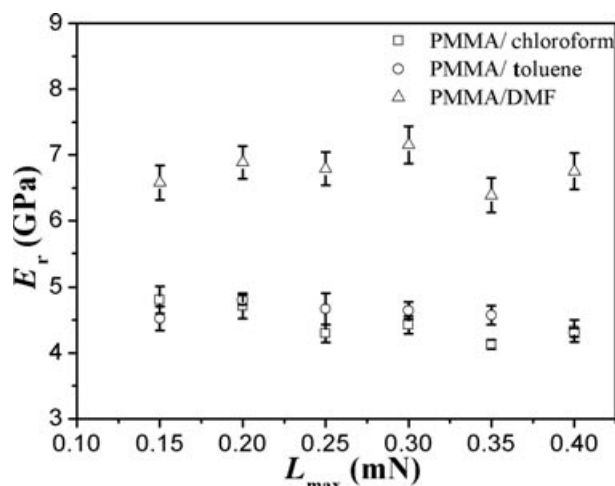


FIGURE 2. Reduced modulus E_r plotted as a function of the different peak load L_{\max} for PMMA/chloroform, PMMA/toluene, and PMMA/DMF samples.

made samples (not reported here) showed no aggregates and flat morphology, with low surface roughness (RMS ~ 3 nm on a $10 \times 10 \mu\text{m}^2$ area).

In Table II, the values of E_r , averaged over all the peak loads for each type of sample are presented.

The $\langle E_r \rangle$ values measured for the PMMA/chloroform and PMMA/toluene samples are very close to each other and comparable to other PMMA E_r values measured by nanoindentation and reported in the literature.^{20,21} The $\langle E_r \rangle$ value for the PMMA/DMF sample is significantly higher, instead.

In Fig. 3, a comparison of creep strain data of the three different PMMA samples is also presented. For each sample, an averaged creep strain value was calculated at the end of the dwell period (60 s) from the set of 10 indentation performed at the peak load $L_{\max} = 150 \mu\text{N}$. A statistical analysis of variance

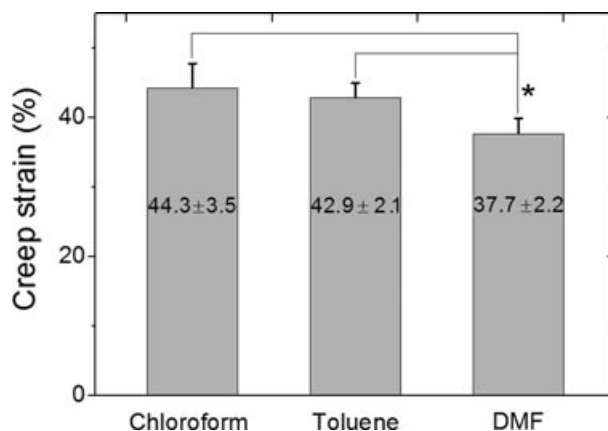


FIGURE 3. ANOVA test comparison of the creep values obtained at the peak load $L_{\max} = 150 \mu\text{N}$ for the PMMA/solvent samples (*: $p < 0.05$).

(ANOVA test) shows that the difference between the PMMA/chloroform and the PMMA/toluene samples is not significant (i.e., the condition for the level of significance, $p < 0.05$, is not met), whereas the PMMA/DMF sample shows a creep strain that is significantly lower ($p < 0.05$) than that of both the PMMA/chloroform and the PMMA/toluene samples.

The highest creep deformation is observed in the PMMA/chloroform sample. In this case, we could expect that the acrylate groups strongly bond the Cl atoms, keeping the volatile solvent trapped within the polymer chains and giving rise to the plasticizing effect. In the case of PMMA/toluene, a weak PMMA/solvent reaction is likely to occur, because of the lower polarity and the lower level of H-bonding interaction with the chains when compared to chloroform (see Table I), which might justify a slightly lower creep value. For the PMMA/DMF sample, the creep is definitely lower than for both chloroform and toluene samples, because of the strong H bonding of the solvent molecules with the carbonyl groups of PMMA. The H bonds, when present, have a bridging effect on the polymer, which can probably explain the much higher reduced modulus observed in the PMMA/DMF sample with respect to that of the other PMMA/solvent samples.

TABLE II
Average Value of Reduced Modulus (E_r) and the Respective Standard Deviation for the Three Types of Samples Are Reported

Sample	Quantity	
	$\langle E_r \rangle$ (GPa)	Standard Deviation (GPa)
PMMA/chloroform	4.4	0.3
PMMA/toluene	4.6	0.2
PMMA/DMF	6.8	0.3

FTIR ANALYSIS

Figures 4a–c show in the main window the synoptic plots of the room temperature infrared spectra of the PMMA powder, the bare solvent, and the

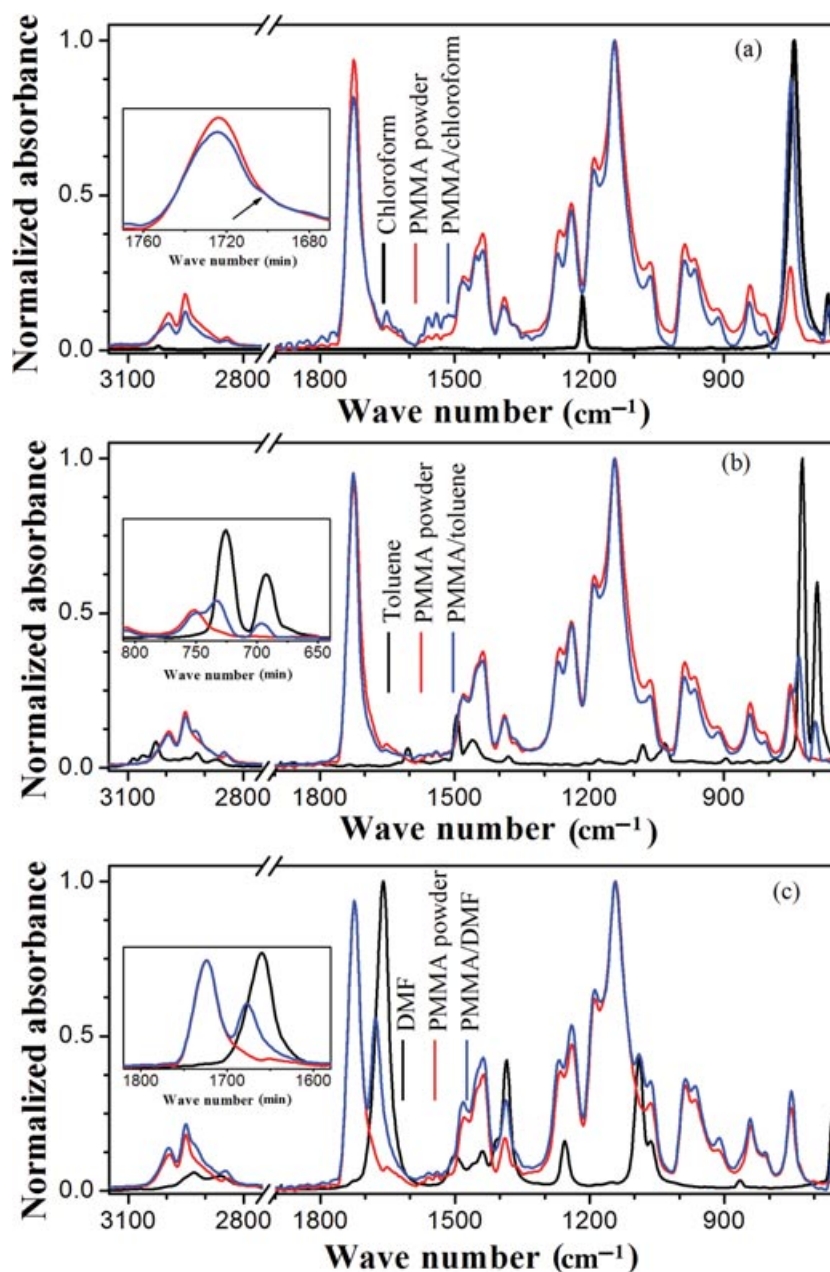


FIGURE 4. FTIR spectra of the PMMA powder and, for each panel, bare solvent, and PMMA/solvent sample for (a) chloroform, (b) toluene, and (c) DMF solvent, respectively. The insets shows closeups of peculiar spectral regions.

PMMA sample prepared from the solvent. Thus in each panel the line shows the same PMMA powder spectrum, to be compared with the PMMA/solvent sample spectrum.

In the PMMA spectrum, the following characteristic features appear due to the polymer structure: the stretching peak of C=O in carbonyl groups at 1725 cm^{-1} ; the peaks of the bend vibration of $-\text{CH}_2$

and $-\text{CH}_3$ groups at 1450 and 1388 cm^{-1} , respectively; the peaks of the stretching vibration of the C–O–C and C–H groups at $1100\text{--}1200\text{ cm}^{-1}$ and $3000\text{--}2840\text{ cm}^{-1}$, respectively.²²

Furthermore, several more peaks can be found due to the possible different tacticities of PMMA. In particular, the three absorption peaks at 751 , 910 , and 1063 cm^{-1} are attributed to the syndiotactic

PMMA structure.²³ However, the steric hindrance of the substituted group $-\text{COOCH}_3$ on the PMMA chain makes the C–C in the end of growing chain rotate, which is helpful to form syndiotactic and atactic structures.

Figure 4a shows the FTIR spectra for the case of the chloroform solution. A closeup of the carbonyl band centered at 1725 cm^{-1} is shown in the inset. It can be seen that at 1700 cm^{-1} a weak shoulder (see arrow) appears inside the band of the PMMA/chloroform sample with respect to the PMMA powder. This is reasonably due to the hydrogen bonding directly to the carbonyl fraction. However, this does not affect the band center position.

Figure 4b shows the FTIR spectra for the case of the toluene solution. In this case, as shown in the inset, close to the PMMA syndiotactic peak at 751 cm^{-1} two new peaks appear in the toluene-casted PMMA at ~ 733 and $\sim 696\text{ cm}^{-1}$, as a result of the interaction between toluene and PMMA. Compared to the original peaks in the toluene, the peaks in PMMA/toluene are shifted toward higher wave numbers, probably due to molecular movement and group rotation. Furthermore, the PMMA powder band at 2848 cm^{-1} in the figure main window is shifted to 2872 cm^{-1} . This can be a consequence of the steric hindrance effect, which is higher for toluene, thus leading to hindering the molecular interactions inside the PMMA chains.

Figure 4c shows the FTIR spectra for the case of the DMF solution. Compared to the spectra of the other solvents (Figures 4a and 4b), and the DMF spectrum (Fig. 4c) shows a large number of distributed peaks in the intermediate spectral region of $1000\text{--}1800\text{ cm}^{-1}$. Along with this, it can be seen that the PMMA/DMF sample peaks are generally slightly broader than the respective peaks for the PMMA powder, opposite than the previous cases (Figs. 4a and 4b). This reflects the previously mentioned interaction of the PMMA chains with the solvent molecules. The spectral region mentioned above is probably correlated to the interaction of DMF amide groups with the methyl group. In particular, it appears clearly in the inset that a strong absorption due to the C=O vibration in DMF at 1660 cm^{-1} is highly coupled into the PMMA carbonyl band at 1725 cm^{-1} . As a result, a new peak appears in the PMMA spectrum at 1677 cm^{-1} .

From the spectra in Fig. 4, the syndiotactic content of the solution-casted PMMA samples was evaluated, by calculating the ratio of the absorption intensities of the peaks at 751 and 1388 cm^{-1} , A_{751}/A_{1388} ; see Table III. It can be seen that the PMMA/toluene

TABLE III
Ratio of the Intensity of the Absorption Peaks at 751 and 1388 cm^{-1} , as Extracted from Fig. 4

Sample	A_{751}/A_{1388}
PMMA powder	1.565
PMMA/chloroform	6.014
PMMA/toluene	1.540
PMMA/DMF	1.126

sample maintains a degree of syndiotacticity close to that of the PMMA powder. On the contrary, the stereostructure of the PMMA/chloroform sample shows a much higher syndiotacticity, whereas the syndiotacticity of the PMMA/DMF film is only slightly decreased with respect to the PMMA powder.

CONCLUSION

In this work, the effect of using chloroform, toluene, and DMF solvents in the preparation of solution-casted PMMA samples was addressed. Sensitive techniques such as DSC for the detection of the glass transition in the PMMA samples, nanoindentation for the measurement of the mechanical properties, and FTIR spectroscopy for detecting the structural changes were employed in combination. Both the thermal and mechanical properties of the PMMA samples appear to be strongly influenced by the choice of the solvent used for the preparation, due to its polarity and to its capability of forming H bonds with the polymer. In particular, for the PMMA samples prepared from chloroform and toluene solutions the glass transition temperature was $20\text{--}25^\circ\text{C}$ below that of bulk PMMA, whereas for the PMMA samples prepared from DMF solution it was $\sim 10^\circ\text{C}$ above. The PMMA samples prepared from the DMF solution also showed higher reduced modulus and lower creep effect with respect to the samples prepared from chloroform and toluene solutions. The spectroscopic analysis provided a comprehensive picture of the structural changes that underwent in the PMMA samples and allowed to assign the above-observed thermal and mechanical effects to the different hydrogen bonding contribution of the solvents to the polymer chain rigidity. Specifically, a polymer chain distortion caused the weakening in the samples prepared from chloroform and toluene solutions,

whereas a bonding between polymer carbonyl and solvent amide groups caused the strengthening in the samples prepared from the DMF solution.

References

1. Chen, L. M.; Shen, K. Z. *J Appl Polym Sci* 2000, 78, 1906–1910.
2. Chen, L. M.; Shen, K. Z. *J Appl Polym Sci* 2000, 78, 1911–1971.
3. Fukushima, H.; Ogino, Y.; Matsuba, G.; Nishida, K.; Kanaya, T. *Polymer* 2005, 46, 1878–1885.
4. Walsh, C.; Franses, E. *Thin Solid Films* 2003, 429, 71–76.
5. Briscoe, B. J.; Akram, A.; Adams, M. J.; Johnson, S. A.; Gorman, D. M. *J Mater Sci* 2002, 37, 4929–4936.
6. Haller, I.; Hatzakis, M.; Srinivasan, R. *IBM J Res Develop* 1968, 12, 251–256.
7. Burke, B.; Herlihy, T., Jr; Spisak, A.; Williams, K. *Nanotechnology* 2008, 19, 215301–215306.
8. Chou, S. Y.; Krauss, P. R.; Renstrom, P. *J Appl Phys Lett* 1995, 67, 3114–3116.
9. D'Amore, F.; Lanata, M.; Pietralunga, S.; Gallazzi, M.; Zerbi, G. 2004, 24, 661–665.
10. Sciancalepore, C.; Cassano, T.; Curri, M.; Mecerreyes, D.; Valentini, A.; Agostiano, A.; Tommasi, R.; Striccoli, M. *Nanotechnology* 2008, 19, 205705–205712.
11. Bistac, S.; Schultz, J. *Int J Adhes Adhes* 1997, 17, 197–201.
12. Feng, X.; Weiwen, F.; Rongshi, C. *Chem China* 2006, 1, 45–47.
13. Hong, P. D.; Huang, H. T.; Chou, C. M. *Polym Int* 2000, 49, 407–411.
14. Bubb, D. M.; Papantonakis, M.; Collins, B.; Brookes, E.; Wood, J.; Gurudas, U. *Chem Phys Lett* 2007, 448, 194–197.
15. Kaczmarek, H.; Chaberska, H. *Polym Testing* 2008, 27, 736–742.
16. Hansen, C. *Hansen Solubility Parameters: A User's Handbook*, 2nd ed.; CRC Press: Boca Raton, FL; 2007.
17. ASTM. *Instrumented indentation testing and designation*. E2546-07, 2007.
18. Fischer-Cripps, A.C. *Nanoindentation*; Springer: New York, 2004.
19. Rau, K.; Singh, R.; Goldberg, E. *Mater Res Innovations* 2002, 5, 151–161.
20. Briscoe, B.; Sebastian, K. S. *Proc R Soc, A: Math Phys Sci* 1996, 452, 439–457.
21. Hochstetter, G.; Jimenez, A.; Cano, J. P.; Felder, E. *Tribol Int* 2003, 36, 973–985.
22. Vien, D. L.; Colthup, N. B.; Fateley, W. G.; Grasselli, J. G. *The Handbook of Infrared and Raman Characteristic Frequencies of Organic Molecules*; Academic Press: New York, 1991.
23. Brandrup, I. *Polymer Handbook*, 4th ed.; Wiley Interscience: New York, 1999.